Selective and Efficient Quantum Process Tomography for Non-Trace-Preserving Maps: Implementation with a Superconducting Quantum Processor

Q. Pears Stefano[1,2,*] I. Perito[1] and L. Rebón[3]

[1]*Departamento de Física, FCEyN, Universidad de Buenos Aires, Buenos Aires, Argentina*
[2]*Consejo Nacional de Investigaciones Científicas y Técnicas (CONICET), Argentina*
[3]*Departamento de Física, IFLP - CONICET, Universidad Nacional de La Plata, C.C. 67, La Plata 1900, Argentina*

Alternatively to the full reconstruction of an unknown quantum process, the so-called selective and efficient quantum process tomography (SEQPT) allows estimating, individually and up to the required accuracy, a given element of the matrix that describes such an operation with a polynomial amount of resources. The implementation of this protocol has been carried out with success to characterize the evolution of a quantum system that is well described by a trace-preserving quantum map. Here, we deal with a more general type of quantum process that does not preserve the trace of the input quantum state, which naturally arises in the presence of imperfect devices and system-environment interactions, in the context of quantum information science or quantum dynamics control. In that case, we show with the aid of *a priori* information on the losses structure of the quantum channel that the SEQPT reconstruction can be adapted to reconstruct the non-trace-preserving map. We explicitly describe how to implement the reconstruction in an arbitrary Hilbert space of finite dimension d. The method is experimentally verified on a superconducting quantum processor provided by IBM Quantum services, by estimating several non-trace-preserving quantum processes in dimensions up to $d = 6$. Our results show that it is possible to efficiently reconstruct non-trace-preserving processes, with high precision, and with significantly higher fidelity than when the process is assumed to be trace preserving.

I. INTRODUCTION

Characterizing the temporal evolution of quantum systems is a crucial task not only used to quantitatively describe naturally occurring processes, but also for certifying the correct functioning of any device that performs quantum information protocols, like those designed for quantum computing and cryptography, among others [1–5]. The different strategies to achieve this task are usually known as *quantum process tomography* (QPT) protocols [6–8]. Given that quantum channels are linear maps, standard QPT schemes based on a linear inversion method [9] are conceptually simple but inefficient in practice, as they require an amount of resources that scales exponentially with the size of the system under study. However, protocols that are both selective (they allow partial information about the channel to be obtained without the need to completely reconstruct it) and efficient (the number of required measurements increases with the desired precision but does not depend on the size of the system) have been theoretically developed [10,11] and experimentally tested [12–15]. These protocols make use of particular sets of states known as uniform 2-designs [16]. One easy way to construct such a set is from the elements of a complete set of mutually unbiased bases (MUBs) [17,18], which are only known to exist in Hilbert spaces whose dimension is the power of a prime number [19–21]. More recently, selective and efficient quantum process tomography (SEQPT) protocols that, by making use of complete sets of MUBs in auxiliary Hilbert spaces, can be easily implemented in any dimension were presented in Ref. [22], while its experimental utility has been shown on a photonic platform [23].

All the protocols named above are designed to describe quantum processes that preserve the trace of the quantum input state, but, in general, one has to deal with open quantum systems, where the evolution is not necessarily described by a trace-preserving quantum map. Even when the quantum process we intend to describe is, theoretically, a trace-preserving map, real-world quantum channels or devices have inherent losses. Thus, a generalization of the previous schemes to reconstruct non-trace-preserving processes is required. As an example, in Ref. [24], we can observe the need to resort to QPT methods for non-trace-preserving maps, to characterize quantum algorithms implemented in a four-qubit superconducting quantum processor. In other cases, the quantum algorithms are implemented in a probabilistic platform. This is the case

---

*Corresponding author. quimeyps@df.uba.ar

of the Knill-Laflamme-Milburn linear-optic quantum computing scheme [25,26], where the inherent probabilistic nature of the implementation makes the complete process a non-trace-preserving one [27,28].

In this work, we show that, when some *a priori* information about losses in a given channel is at hand, a generalization of the SEQPT protocols to reconstruct such a non-trace-preserving channel can be obtained. Additionally to a detailed description of the proposed scheme that works for Hilbert spaces of arbitrary finite dimension, we test its validity by performing the experimental reconstruction of non-trace-preserving quantum processes in dimensions $d = 3$ and $d = 6$ in ibmq_lima (a five-qubit quantum processor) provided by IBM Quantum services [29]. To this end, we propose an encoding that embeds the d-dimensional Hilbert space in the n-qubit-based processor. Namely, we codify the quantum systems of dimensions (qudits) $d = 3$ and $d = 6$ into a two-qubit (dimension $2^2 = 4$) or a three-qubit system (dimension $2^3 = 9$), respectively, using the remaining subspace to introduce a controlled loss. While there are several examples of quantum algorithms implemented in a qubit-based superconducting quantum processor [30–32], including quantum tomography schemes and a recent SEQPT implementation for trace-preserving maps [15], we show that these platforms are also suitable to implement and validate quantum algorithms and tasks for *qudits* of *arbitrary dimensions*.

The paper is organized as follows. In Sec. II we start by reviewing the standard formulation of the SEQPT (Sec. II A). In Sec. II B we introduce the proposed generalization of the method when the process to be characterized does not preserve trace. The details of our experimental implementation on an IBM quantum computer for different quantum processes acting on systems of dimensions $d = 3$ and $d = 6$ are presented in Sec. III. In Sec. IV we show and discuss the obtained results, and finally we conclude with the outstanding aspects of the work in Sec. V.

II. FORMALISM

We start this section by briefly reviewing the formalism to describe a quantum process, followed by the standard formulation of the SEQPT protocol introduced in Refs. [10,11]. It is said that this is *selective*, in the sense that it allows a particular coefficient of the process matrix χ to be obtained without having to perform the full QPT, and *efficient*, since such a coefficient can be determined with subexponential resources. Then, we present its generalization to reconstruct non-trace-preserving quantum processes.

A quantum process can be mathematically represented by a linear and completely positive map $\mathcal{E}$, from the set of density operators into itself [9]. The effect of this map on a quantum state ρ can always be written as a Kraus decomposition $\mathcal{E}(\rho) = \sum_k A_k \rho A_k^\dagger$, where $\{A_k\}_k$ is a set of

linear operators that acts on a Hilbert space $\mathcal{H}$, and satisfies the relation $\sum_k A_k A_k^\dagger \leq \mathbb{I}$ [33]. This restriction implies that $0 \leq \text{Tr}[\mathcal{E}(\rho)] \leq 1$ for any ρ, which guaranties that $\mathcal{E}$ represents a *physical* quantum process. In order to relate the decomposition of the map with measurable parameters, one can choose a convenient basis of operators $\{E_i, i = 0, \ldots, d^2 - 1\}$ with d the dimension of the quantum system, and write each operator A_k in this basis. Therefore, the action of the process is expressed as $\mathcal{E}(\rho) = \sum_{ij} \chi_j^i E_i \rho E^j$ with χ a Hermitian and positive $d^2 \times d^2$ matrix, where we have adopted the convention $E^j \equiv E_j^\dagger$. Now, the trace condition is given by the inequality

$$\sum_{ij} \chi_j^i E^j E_i \leq \mathbb{I}, \tag{1}$$

and it is said that the evolution of the system, under the considered process, is described by a *trace-preserving* or a *non-trace-preserving* map, depending on whether or not the equality is fulfilled. Hence, determining all the coefficients χ_j^i is equivalent to completely characterizing the process.

A. SEQPT for trace-preserving maps

Let us review the standard SEQPT protocol for *trace-preserving* maps. The key quantity for *selectively* reconstructing the process matrix χ is the *average survival probability* $\bar{F}(\mathcal{E}_j^i)$, which can be defined as

$$\bar{F}(\mathcal{E}_j^i) = \int_{\mathcal{H}} d\psi \ \langle\psi|\mathcal{E}(E^i|\psi\rangle\langle\psi|E_j)|\psi\rangle, \tag{2}$$

and it is directly related to the coefficient χ_j^i by the expression

$$\chi_j^i = \frac{d+1}{d}\bar{F}(\mathcal{E}_j^i) - \frac{1}{d^2}\text{Tr}\left[\left(\sum_{\mu\nu}\chi_\mu^\nu E^\nu E_\mu\right)E^i E_j\right]. \tag{3}$$

Since the equality in Eq. (1) is fulfilled, the second term in the previous expression is reduced to $\delta_j^i/(d+1)$ when the summation is performed, and we arrive at the uncoupled equation

$$\chi_j^i = \bar{F}(\mathcal{E}_j^i)\frac{d+1}{d} - \frac{\delta_j^i}{d}, \tag{4}$$

which allows any matrix coefficient χ_j^i to be related to the determination of a single average survival probability.

In order to experimentally estimate $\bar{F}(\mathcal{E}_j^i)$, the integral can be replaced with an average over a particular finite set
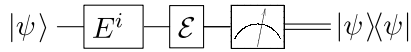
FIG. 1.   Circuit schematic for measuring the survival probability of state $|\psi\rangle$ through the modified channel $\mathcal{E}_i^i$. By sampling over $|\psi\rangle$ in the state 2-design X, we can estimate the diagonal element χ_i^i, corresponding to the process matrix of $\mathcal{E}$.

of states known as a *uniform* 2-design [34]:

$$\bar{F}(\mathcal{E}_j^i) = \frac{1}{N} \sum_{m=1}^{N} \langle\psi_m|\mathcal{E}(E^i|\psi_m\rangle\langle\psi_m|E_j)|\psi_m\rangle. \quad (5)$$

Note that the term on the right-hand side of Eq. (5) has a clear experimental interpretation: it represents the survival probability through a modified channel $\mathcal{E}_j^i$, averaged over X. For example, the diagonal coefficient χ_i^i can be obtained by preparing all the states in X, one by one, and measuring their survival probabilities through the modified channel $\mathcal{E}_i^i$, as schematized in Fig. 1. In the nondiagonal case, the modified channel $\mathcal{E}_j^i$ is not physical, but the coefficient χ_j^i can still be obtained from the outputs of *at most* four of those circuits (see Appendix A).

The problem of finding a state 2-design is easily solved when the dimension d of the system is the power of a prime number. In this case, it is always possible to construct a complete set of MUBs [20] that automatically constitutes an uniform 2-design [18]. In other cases it is not trivial to compute the integral in Eq. (2) as an average over a finite set of states, and thus the protocol becomes impractical. However, the generalization of the MUBs-based SEQPT protocol to quantum processes in a Hilbert space of arbitrary dimension d has been developed in Ref. [22], and experimentally implemented in Ref. [23], for the case of trace-preserving maps. The approach exploits the fact that tensor products of 2-designs can be used to approximate a state 2-design [35]. Then, since an arbitrary dimension d can always be factorized into power-of-prime numbers, i.e., $d = p_1^{n_1} p_2^{n_2} \cdots p_N^{n_N}$ with $\{p_i\}_{i=1}^{N}$ all different prime numbers, the tensor product of maximal sets of MUBs in Hilbert spaces of dimensions $D_1 = p_1^{n_1}$, $D_2 = p_2^{n_2}, \ldots, D_N = p_N^{n_N}$ provides a good approximation for integration purposes.

To fix ideas, we briefly describe the bipartite case, where the dimension of the Hilbert space is factorized as $d = D_1 D_2$, but the extension to any other multipartite case is straightforward [22]. A more thorough explanation, already presented in Ref. [22], can be followed in Appendix B. We start by expanding the map $\mathcal{E}$ over $\mathcal{H}$ ($\mathcal{H} = \mathcal{H}_1 \otimes \mathcal{H}_2$), in a basis that is a tensor product of operators acting on $\mathcal{H}_1$ and $\mathcal{H}_2$, being $D_1 = p_1^{n_1} = \dim(\mathcal{H}_1)$ and $D_2 = p_1^{n_2} = \dim(\mathcal{H}_2)$, respectively. This basis can be chosen as tensor products of two orthogonal operator bases $\{E_{j_1 j_2} \equiv E_{j_1} \otimes E_{j_2}\}_{j_1=0,\ldots,D_1^2-1}^{j_2=0,\ldots,D_2^2-1}$, where
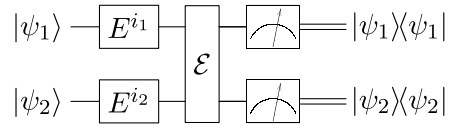

FIG. 2.   Circuit schematic to perform SEQPT when the dimension of the Hilbert space can be factorized as powers of two prime numbers. By sampling over the product 2-design $X_\otimes$, with the survival probability of state $|\psi\rangle = |\psi_1\rangle \otimes |\psi_2\rangle$ through the modified channel $\mathcal{E}_{i_1 i_2}^{i_1 i_2}$ as output, we can estimate the diagonal element $\chi_{i_1 i_2}^{i_1 i_2}$ corresponding to the process matrix of $\mathcal{E}$.

each element E_{j_i} ($i = 1, 2$) is a unitary matrix. Hence, we are able to rewrite $\mathcal{E}$ as

$$\mathcal{E}(\rho) = \sum_{\mu_1 \mu_2 \nu_1 \nu_2} \chi_{\nu_1 \nu_2}^{\mu_1 \mu_2} E_{\mu_1 \mu_2} \rho E^{\nu_1 \nu_2} \quad (6)$$

for some coefficients $\chi_{\nu_1 \nu_2}^{\mu_1 \mu_2}$. Furthermore, we can easily define a uniform 2-design X_1 (X_2), based on MUBs, for the Hilbert space $\mathcal{H}_1$ ($\mathcal{H}_2$).

Now, the survival probability is evaluated, experimentally, for states belonging to $X_\otimes = \{|\psi_1\rangle \otimes |\psi_2\rangle$ for $|\psi_1\rangle \in X_1, |\psi_2\rangle \in X_2\}$, that is, the set of all tensor products of an element of X_1 and an element of X_2. Although the average with this sampling scheme does not directly yield $\bar{F}(\mathcal{E}_{j_1 j_2}^{i_1 i_2})$, it allows us to estimate three related average quantities, $\bar{F}_\otimes(\mathcal{E}_{j_1 j_2}^{i_1 i_2})$, $\bar{F}_1(\mathcal{E}_{j_1 j_2}^{i_1 i_2})$, and $\bar{F}_2(\mathcal{E}_{j_1 j_2}^{i_1 i_2})$ (see Appendix B), that can be exactly related to the average survival probability:

$$\bar{F}(\mathcal{E}_{j_1 j_2}^{i_1 i_2}) = \frac{1}{d+1}\left\{\bar{F}_\otimes(\mathcal{E}_{j_1 j_2}^{i_1 i_2})(D_1 + 1)(D_2 + 1)\right.$$
$$+ \frac{2}{d}\text{Tr}\left[\left(\sum_{\mu\nu} \chi_\mu^\nu E^\nu E_\mu\right)E^i E_j\right]$$
$$\left. - \bar{F}_1(\mathcal{E}_{j_1 j_2}^{i_1 i_2})(D_1 + 1) - \bar{F}_2(\mathcal{E}_{j_1 j_2}^{i_1 i_2})(D_2 + 1)\right\}. \quad (7)$$

An example circuit for this case is depicted in Fig. 2. This measurement corresponds to the reconstruction of a given diagonal coefficient $\chi_{i_1 i_2}^{i_1 i_2}$. Here, an arbitrary state $|\psi\rangle = |\psi_1\rangle \otimes |\psi_2\rangle$ in $X_\otimes$ is prepared and its survival probability through the modified channel $\mathcal{E}_{i_1 i_2}^{i_1 i_2}$ is obtained as output. Finally, as in the case of the power-of-prime dimension, if a trace-preserving map is assumed, from Eq. (7), an expression for any $\chi_{j_1 j_2}^{i_1 i_2}$ totally uncoupled to the other elements of the process matrix is obtained.

B. SEQPT formulation for non-trace-preserving maps

The assumption of the trace-preserving property of map $\mathcal{E}$ is essential to achieve *selectivity* in the tomographic method. If we drop this assumption, Eq. (3) can no longer

be decoupled to obtain Eq. (4). Thus, each matrix coefficient χ_j^i is coupled to all the others, and of the order of about d^4 circuits, like that in Fig. 1, should be performed to solve the resulting equation system. However, with some *a priori* information about the process to be characterized, this issue could be overcome. Indeed, it can be done by defining a semidefinite positive Hermitian operator $\mathcal{P}$, given by

$$\mathcal{P} = \sum_{ij} \chi_j^i E^j E_i. \tag{8}$$

This operator was originally introduced in Ref. [36], in the context of standard quantum process tomography (SQPT) for non-trace-preserving maps. It encodes the losses of the system, so that, given an input state ρ, the probability of obtaining an output state after process $\mathcal{E}$ (probability of success of the process) is

$$\text{Tr}[\mathcal{E}(\rho)] = \text{Tr}[\mathcal{P}\rho]. \tag{9}$$

The meaning of $\mathcal{P}$ becomes clear when it is analyzed in its diagonal form: let us write $\mathcal{P} = \sum_i \gamma_i |\gamma_i\rangle\langle\gamma_i|$, where the $|\gamma_i\rangle$ are the eigenstates and $0 \leq \gamma_i \leq 1$ the corresponding eigenvalues. Hence, state $|\gamma_i\rangle$ has a probability of success equal to γ_i. For a trace-preserving map, $\gamma_i = 1$ for all i and $\mathcal{P} = \mathbb{I}$. Otherwise, we have a non-trace-preserving process with state-independent ($\gamma_i = \gamma < 1$ for all i) or state-dependent (at least one $\gamma_i < 1$ and different to the others) success probability. For example, in a photonic experiment, this decrease in the trace value may be associated with a global loss, when $\mathcal{P} = \gamma\mathbb{I}$, or to different losses in each path of the setup, in another case. Then, provided that we can have a description of $\mathcal{P}$ as an a priori information of the process, which is possible in many realistic scenarios, Eq. (3) now reduces to

$$\bar{F}(\mathcal{E}_j^i) = \frac{d^2\chi_j^i + \text{Tr}[\mathcal{P}E^iE_j]}{d(d+1)}, \tag{10}$$

and any element χ_j^i can be independently computed from the corresponding average fidelity $\bar{F}(\mathcal{E}_j^i)$. In the particular case in which $\mathcal{P}$ is a multiple of the identity operator, Eq. (10) returns to Eq. (4) but modified by an additive factor $(1-\gamma)\delta_j^i/d$. So, this derivation also includes trace-preserving maps where $\gamma = 1$.

In the bipartite case, the uncoupled expression for element $\chi_{j_1j_2}^{i_1i_2}$ is (the complete derivation is given in Appendix C)

$$\chi_{j_1j_2}^{i_1i_2} = \bar{F}_\otimes(\mathcal{E}_{j_1j_2}^{i_1i_2})\frac{(1+D_1)(1+D_2)}{d}$$
$$+ \frac{1}{d^2}\text{Tr}(\mathcal{P}E^{i_1i_2}E_{j_1j_2}) - \bar{F}_1(\mathcal{E}_{j_1j_2}^{i_1i_2})\frac{1+D_1}{d}$$
$$- \bar{F}_2(\mathcal{E}_{j_1j_2}^{i_1i_2})\frac{1+D_2}{d}. \tag{11}$$

In general, a possible shortcoming of a non-trace-preserving formulation is that previous knowledge of the $\mathcal{P}$ matrix is needed. However, there are several use cases where that requirement is available. For example, when the losses of each individual building block of a quantum circuit are characterized, $\mathcal{P}$ could be estimated *a priori* for each particular configuration of the full circuit. Therefore, the implementation of the SEQPT scheme is suitable to certify the correct implementation and the performance of the algorithm of interest (see, for example, Ref. [24]). In a similar way, the implementation of nondeterministic quantum gates [25,26,37] could be tested by the method that we present in this work.

It should be mentioned that, if the reconstruction of the quantum map is carried out assuming, incorrectly, that the trace is preserved, the fidelity will drop with respect to the reconstruction, assuming that the trace is not preserved (see our results in Sec. IV B), and this difference tends to increase with losses [36]. Furthermore, the topic of QPT schemes for non-trace-preserving maps is seldom treated in the literature. The SQPT method works off the shelf [36,38] but lacks efficiency, given that it requires a number of measurements that grow exponentially with the dimension of the system. Other approaches are (i) direct characterization of quantum dynamics [7], which requires an ancillary state, (ii) the use of coherent states [27], and (iii) QPT via weak values [39]. In that regard, the generalization of SEQPT to non-trace-preserving processes raises the possibility of performing efficient and selective tomography for this type of map.

Finally, it is important to mention that if we have no knowledge of $\mathcal{P}$, Eq. (9) can be used to gain partial information about it, by measuring the probability of success in some selected basis. For example, by just sampling states of the 2-design, all the diagonal elements of the $\mathcal{P}$ matrix can be estimated. We think that, as future work, it is worth exploring whether this partial information of $\mathcal{P}$ can be combined with optimization methods, or even with variations of SEQPT that simultaneously estimate any diagonal coefficient of the process matrix χ, not a single one (generalization I in Ref. [11]), to perform a selective and efficient tomography even in the absence of information about $\mathcal{P}$.

III. EXPERIMENTAL REALIZATION ON AN IBM QUANTUM COMPUTER

To experimentally validate the non-trace-preserving formulation of the SEQPT method, we use the superconducting quantum computer ibmq_lima. This is a freely available quantum processor of five qubits that can be programmed with the open-source PYTHON framework Qiskit [40]. We implement the SEQPT to characterize a non-trace-preserving quantum process for both $d = 3$, a dimension with a known 2-design, and $d = 6$, the minimal dimension in which the bipartite extension is non trivial.

A. Reconstruction of quantum processes in $d = 3$

To represent a three-dimensional quantum system (qutrit) on a qubit-based quantum computer, we use two qubits of the processor, with

$$|00\rangle \equiv |0\rangle_3, \qquad |10\rangle \equiv |2\rangle_3,$$

$$|01\rangle \equiv |1\rangle_3, \qquad \underbrace{|11\rangle \equiv |\ell\rangle,}_{\text{loss state}} \qquad (12)$$

where $\mathcal{B} = \{|q_1 q_0\rangle\}_{q_j=0,1}$ is the computational basis for the two-qubit system and $\mathcal{B}' = \{|k\rangle_3\}_{k=0,\dots,2}$ is the canonical basis for the three-dimensional Hilbert space $\mathcal{H}^{(3)}$. It is important to mention that, since there is one more state in the basis of a two-qubit system, this extra state should be discarded. We take advantage of this to simulate losses in the qutrit evolution. That is, any unitary transformation that couples subset $\{|00\rangle, |01\rangle, |10\rangle\}$ to the remaining element $|11\rangle \in \mathcal{B}$ will represent a non-trace-preserving process on the Hilbert space defined by $\mathcal{B}'$.

The target qutrit process, $\mathcal{E}^{(3)}$, to be implemented and reconstructed is based on a Hadamard gate extended as a qutrit quantum operation [41]:

$$H_{01} = \frac{1}{\sqrt{2}} \begin{pmatrix} 1 & 1 & 0 \\ 1 & -1 & 0 \\ 0 & 0 & \sqrt{2} \end{pmatrix}. \qquad (13)$$

As can be seen, H_{01} maps the basis states $|0\rangle_3 \to (|0\rangle_3 + |1\rangle_3)/\sqrt{2}$ and $|1\rangle_3 \to (|0\rangle_3 - |1\rangle_3)/\sqrt{2}$, and leaves state $|2\rangle_3$ unchanged. However, since we are interested in the non-trace-preserving process, we include a *beam-splitter-like loss* of 50% affecting state $|2\rangle_3$, which results in a Kraus decomposition with a single unitary operator, $\mathcal{E}^{(3)}(\rho) = A^{(3)} \rho (A^{(3)})^\dagger$, where

$$A^{(3)} = \frac{1}{\sqrt{2}} (|0\rangle\langle 0| - |1\rangle\langle 1| + |2\rangle\langle 2|$$

$$+ |0\rangle\langle 1| + |1\rangle\langle 0|).$$

Hence, losses in the qutrit evolution will correspond to a coupling between state $|2\rangle_3$ and the discarded two-qubit state renamed as $|\ell\rangle$. In basis $\mathcal{B}$, this coupling can be performed by a controlled-Hadamard gate on the target qubit 0, controlled by qubit 1. Figure 3 shows the equivalent circuit that implements such a loss in the IBMQ processor (LOSS 50%). The percentage of loss, $r \times 100$, can be set to a different value by changing the angle of rotation of some of the R_z gates: this allows simulating non-trace-preserving channels, with arbitrary losses, without increasing the depth of the circuit. The schematic of the circuit to implement a *general* beam-splitter-like gate is discussed in Appendix D. Then, it is easy to see that in
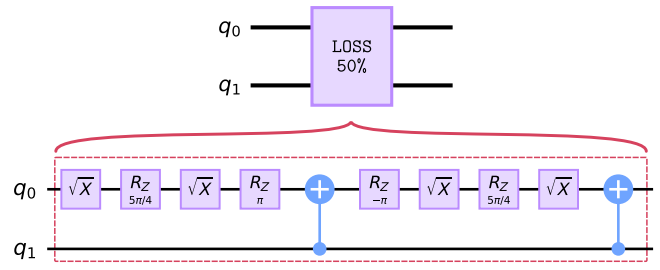

FIG. 3. Circuit to implement a beam-splitter-like loss affecting state $|10\rangle \equiv |2\rangle_3$. This state is coupled to the discarded two-qubit state $|11\rangle \equiv |\ell\rangle$ with a 50% probability.

basis $\mathcal{B}'$ the loss operator $\mathcal{P}$ corresponding to process $\mathcal{E}^{(3)}$ has a diagonal matrix form, i.e.,

$$\mathcal{P} = \begin{pmatrix} 1 & 0 & 0 \\ 0 & 1 & 0 \\ 0 & 0 & \frac{1}{2} \end{pmatrix}, \qquad (14)$$

that is, $\gamma_0 = \gamma_1 = 1$ and $\gamma_2 = r = \frac{1}{2}$. This is the information that we consider (*a priori*) known to reconstruct the process.

At this point, we describe our implementation of the SEQPT protocol in the two-qubit processor. As an example, Fig. 4 shows the schematic circuit, which closely resemble that in Fig. 1, to sample a particular element of the 2-design X through the modified channel $\mathcal{E}_i^i$. As a state 2-design, we choose a complete set of MUBs that in $d = 3$ has exactly 12 elements. The first stage of the circuit in Fig. 4 corresponds to the preparation of the selected input state $|\psi_m\rangle \equiv |\psi_M^J\rangle$, modified by operator E^i, where J ($J = 0, \dots, d$) indicates the MUB and M ($M = 0, \dots, d-1$) refers to a particular state in that J MUB. Because of the selected basis of operators, the resulting state is an element of the same J MUB: $|\psi_{M'}^J\rangle$ (see Appendix E). The second stage corresponds to the circuit that implements process $\mathcal{E}^{(3)}$, while the last stage performs a measurement in the J MUB, required to estimate the survival probability of the sampled state [Eq. (5)]. In the presented example, as the projection is on the canonical basis $\mathcal{B}_{J=0}$, there is no need for a change of basis prior to detection of each qubit.

B. Reconstruction of quantum processes in $d = 6$

To represent a six-dimensional quantum system (qudit), at least three qubits of the IBMQ computer are needed. Furthermore, to implement the bipartite version of the SEQPT, we must factorize $\mathcal{H}^{(6)}$ as $\mathcal{H}_1 \otimes \mathcal{H}_2$, with $d = D_1 D_2 = 2 \times 3$. A suitable alternative is to consider similar decompositions to those in Eq. (12) to expand $\mathcal{H}_2$, and add an extra qubit for $\mathcal{H}_1$:

$$|000\rangle \equiv |0\rangle_6 = |0\rangle_2 \otimes |0\rangle_3, \quad |100\rangle \equiv |3\rangle_6 = |1\rangle_2 \otimes |0\rangle_3,$$

$$|001\rangle \equiv |1\rangle_6 = |0\rangle_2 \otimes |1\rangle_3, \quad |101\rangle \equiv |4\rangle_6 = |1\rangle_2 \otimes |1\rangle_3,$$
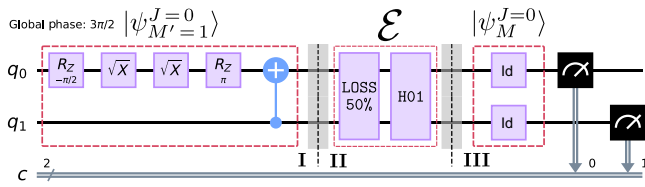
FIG. 4. Example of a circuit that samples an element of the 2-design X, in a Hilbert space of dimension $d = 3$, through the modified channel $\mathcal{E}_i^i$. **I**. In this particular case, the sampled element, after being modified by the corresponding E_i operator, is $|\psi_{M'=1}^{J=0}\rangle$. **II**. The process $\mathcal{E}$ corresponds to a LOSS 50% followed by the operation H01. **III**. In the measurement stage, an unitary transformation (the identity in this example) represents the change of basis from $\mathcal{B}_J$ to the canonical one ($\mathcal{B}_{J=0}$), followed by the measurement of the state of each qubit.

$$|010\rangle \equiv |2\rangle_6 = |0\rangle_2 \otimes |2\rangle_3, \quad |110\rangle \equiv |5\rangle_6 = |1\rangle_2 \otimes |2\rangle_3,$$

$$\underbrace{|011\rangle \equiv |\ell_1\rangle, \qquad |111\rangle \equiv |\ell_2\rangle}_{\text{loss states}} \qquad (15)$$

with $\mathcal{B}'' = \{|q_2 q_1 q_0\rangle\}_{q_j=0,1}$ the computational basis for the three-qubit system and $\mathcal{B}''' = \{|k\rangle_6\}_{k=0,\ldots,5}$ the canonical basis for $\mathcal{H}^{(6)}$. It is worth noting that in this case we have used two states ($|011\rangle$ and $|111\rangle \in \mathcal{B}''$ renamed as $|\ell_1\rangle$ and $|\ell_2\rangle$) to simulate losses in the evolution of the qudit. For this purpose, the same circuit as in Fig. 3 is programmed to implement a beam-splitter-like loss with a 50% chance of coupling $|2\rangle_6$ and $|5\rangle_6$ to the lost states $|\ell_1\rangle$ and $|\ell_2\rangle$, respectively.

The target process that we implement for its subsequent reconstruction can be decomposed as $\mathcal{E}^{(6)}(\rho) = A^{(6)} \rho (A^{(6)})^\dagger$ with

$$A^{(6)} = |0\rangle\langle 0| + |3\rangle\langle 3| + e^{i\pi/3}(|1\rangle\langle 1| + |4\rangle\langle 4|)$$

$$+ \frac{1}{\sqrt{2}}(|2\rangle\langle 5| + |5\rangle\langle 2|). \qquad (16)$$

This corresponds to a phase shift of $\varphi = \pi/3$ affecting states $|1\rangle_6$ and $|4\rangle_6$, a swap operation between states $|2\rangle_6$ and $|5\rangle_6$, and losses that also affect these two states, SWAP25 + LOSS 50%. For this non-trace-preserving process, the diagonal form of the $\mathcal{P}$ matrix is

$$\text{diag}(\mathcal{P}) = \left(1, 1, \tfrac{1}{2}, 1, 1, \tfrac{1}{2}\right), \qquad (17)$$

that is, $\gamma_i = 1$ for $i \in \{0, 1, 3, 4\}$, while $\gamma_i = r = \frac{1}{2}$ for $i \in \{2, 5\}$.

Finally, with the encoding election for a qudit [Eqs. (15)], the SEQPT protocol in the three-qubit processor is implemented by programming the schematic circuit shown in Fig. 5, which resembles the circuit for the bipartite case depicted in Fig. 2. In this example, an element $|\psi_m\rangle \equiv |\psi_{M_1}^{J_1}\rangle \otimes |\psi_{M_2}^{J_2}\rangle$ in the product 2-design $X_\otimes$ is sampled

through the modified channel $\mathcal{E}_{i_1 i_2}^{i_1 i_2}$ and projected to estimate its survival probability [Eq. (B1) in Appendix B]. Both 2-design states, X_1 and X_2, are chosen to be complete sets of MUBs, so that $|\psi_{M_1}^{J_1}\rangle$ and $|\psi_{M_2}^{J_2}\rangle$ are the M_1 and M_2 elements of the J_1 MUB in $D_1 = 2$, and the J_2 MUB in $D_2 = 3$, respectively, giving a total of 72 elements in $X_\otimes$. In the first stage, state $|\psi_m\rangle$ is prepared and modified by operator $E^{i_1 i_2}$ that, analogously to the case $d = 3$, gives, by construction, another element of $X_\otimes$. Thus, the experimental implementation of the modified channel only requires the preparation of elements in $X_\otimes$ as input states of channel $\mathcal{E}^{(6)}$, which corresponds to the second stage of Fig. 5, while the last stage performs a projective measurement on the tensor product of J_1 and J_2 bases.

It is important to mention that, as we will seen in Sec. IV, the particular choice of MUBs as state 2-designs, together with the operator bases used in this work, results in a significant reduction in the number of circuits to be implemented to carry out the SEQPT. An explicit construction of the 2-designs and the operator bases are discussed in Appendix E.

IV. RESULTS AND DISCUSSION

In this section we show the main experimental results obtained when using the SEQPT method in the reconstruction of non-trace-preserving quantum maps. They correspond to quantum circuits with losses for two different dimensions: $d = 3$ (power-of-prime dimension) and $d = 6$ (nontrivial example of arbitrary dimension). In the case of $d = 6$ we also explore, in detail, the selective and efficient properties of the method.

A. Process matrix reconstruction: case $d = 3$

To assess the viability of the SEQPT in the case of non-trace-preserving quantum maps, we first use the method to perform a full tomography of the target channel $\mathcal{E}^{(3)}$. To this end, all of the $9 \times 9 = 81$ coefficients of the expected theoretical process matrix χ_{theo} are reconstructed, by sampling for each coefficient the 12 elements in the state 2-design X. Because of the particular relation between the selected operator basis and the 2-design (Appendix E), many of the circuits needed to perform that sampling are repeated. Thus, the full tomographic reconstruction requires the implementation of only 36 different circuits like that in Fig. 4, out of a total of $81 \times 12 \times 4 = 3888$ circuits. This shows the importance of an adequate choice of the basis of operators for a given state 2-design, in order to avoid redundancy. Each circuit is repeated 8192 times (*shots*) to estimate the frequency distribution of the outcomes and thus infer the corresponding survival probabilities $\bar{F}(\mathcal{E}_j^i)$. Since an important source of error in the circuit evaluation comes from the measurement stage, an error
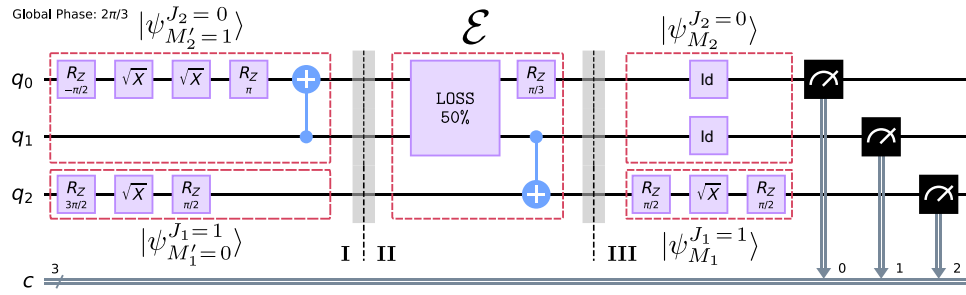
FIG. 5. Example of a circuit that samples an element of the product of 2-designs $X_\otimes = X_1 \otimes X_2$ in a Hilbert space of dimension $d = 6$, through the modified channel $\mathcal{E}_{i_1 i_2}^{i_1 i_2}$. Subspace $\mathcal{H}_1$, whose dimension is $D_1 = 2$, coincides with the third qubit. **I**. The sampled element, after being affected by operator $E_{i_1 i_2}$, is $|\psi_{M'=0}^{J_1=1}\rangle \otimes |\psi_{M'=1}^{J_2=0}\rangle$. **II**. Process $\mathcal{E}$ corresponds to a LOSS 50% followed by the R_z and controlled-NOT gates that implement a SWAP25. **III**. Finally, a unitary transformation is applied to change the basis from $\mathcal{B}_{J_1=1} \otimes \mathcal{B}_{J_2=0}$ to the canonical one ($\mathcal{B}_{J_1=0} \otimes \mathcal{B}_{J_2=0}$), followed by the measurement of each qubit.

mitigation routine is used to postprocess the frequency distribution. This routine, ignis.mitigation.measurement, is provided by the Qiskit framework module, and relies on an initial calibration measurement, performed on the superconducting quantum computer, of the qubit state prepared in the computational basis.

As in most tomographic methods, due to the effect of statistical and systematic errors, the reconstructed channels are not physical [42,43]. For that reason, after a first estimation of matrix χ_{theo} we solve the convex optimization problem [44]

$$\min_{\chi_{\text{opt}}} \quad \|\chi_{\text{raw}} - \chi_{\text{opt}}\|_F \tag{18a}$$

$$\text{such that} \quad \chi_{\text{opt}} \geq 0, \tag{18b}$$

$$0 \leq \text{Tr}\left(\sum_{ij} \chi_{j\,\text{opt}}^{i} E^j E_i \right) = \text{Tr}(\mathcal{P}) \leq d, \tag{18c}$$

where χ_{raw} is the process matrix experimentally reconstructed using the SEQPT method and χ_{opt} the resulting optimized matrix. This optimization is similar to that used in Ref. [15], where the optimized matrix is the closest matrix, in the sense of the Frobenious norm, to that estimated by the tomographic method, subject to the constraints of physicality. These constraints are as follows: (i) the matrix must be *semidefinite positive*, which in turn implies that the quantum map is complete positive [43]; (ii) the condition on the trace, which ensures a nonincreasing trace map, whose value must be equal to the trace of the $\mathcal{P}$ matrix, is *a priori* known. For lossless evolution, we have $\mathcal{P} \equiv \mathbb{I}$, and the last constraint reduces to the usual one for a trace-preserving quantum map, $\text{Tr}(\sum_{ij} \chi_{j\,\text{opt}}^{i} E^j E_i) = d$.

Figure 6 shows the bar plots representing the real and imaginary parts of the reconstructed process matrix,

$\chi_{\text{expt}} \equiv \chi_{\text{opt}}$ for the channel HO1+LOSS 50%. For comparison reasons, we also show the real and imaginary parts of χ_{theo} (see the upper insets in Fig. 6). As a figure of merit of the reconstruction process, we use the normalized process fidelity

$$\mathcal{F} \equiv \mathcal{F}(\chi_{\text{theo}}, \chi_{\text{expt}}) = \frac{\text{Tr}[\sqrt{\sqrt{\chi_{\text{theo}}}\,\chi_{\text{expt}}\sqrt{\chi_{\text{theo}}}}]}{\sqrt{\text{Tr}[\chi_{\text{theo}}]}\sqrt{\text{Tr}[\chi_{\text{expt}}]}}. \tag{19}$$

This definition acts as a geometric distance in the space of density matrices and, due to the Choi-Jamiołkowski isomorphism [8], it can be used as a geometric distance measure between quantum processes. It should also be noted that the normalization factor is included so that it is $\mathcal{F} = 1$ for identical processes, even when they are non-trace-preserving [24,36].

The resulting fidelity value for process $\mathcal{E}^{(3)}$ is $\mathcal{F}_{\text{SEQPT}} = 0.956$. For completeness, we also reconstruct the process under the SQPT method. Briefly, the SQPT that is conducted on the IBMQ superconducting quantum processor consists of preparing about d^2 states that are a combination of states in the d-dimensional canonical basis: $|k\rangle$, $|k\rangle + |k'\rangle$, and $|k\rangle + i|k'\rangle$, with $k = 0, \dots, d-1$ and $k' = (k+1), \dots, d-1$. Each of these states is then reconstructed, after being affected by the quantum process, through a standard quantum state tomography (QST). The circuits are implemented using the state_tomography_circuits function, provided by the Qiskit Ignis library. As the QST method provided by this framework works for n-qubit states, we then project the resulting reconstructed state onto the three-dimensional subspace of interest. Finally, the linear relation between the prepared and reconstructed states is inverted to obtain the process matrix. The experimental estimation of χ_{theo} under the SQPT results in a process fidelity $F_{\text{SQPT}} = 0.974$, which is slightly higher than that obtained with the SEQPT. However, it should be noted that the implementation of SQPT requires 81
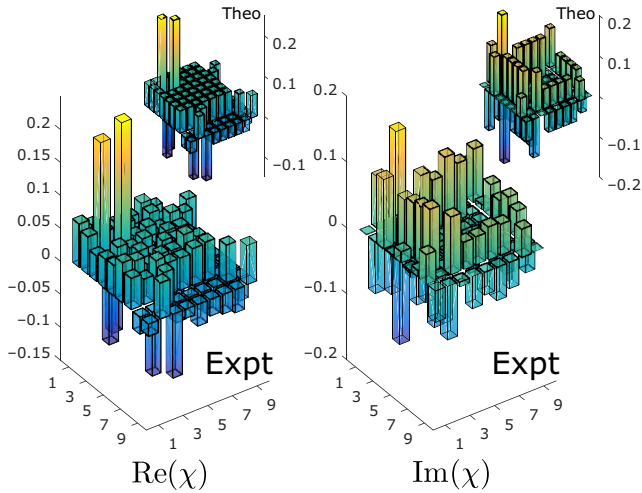
FIG. 6. Comparison of the real (left panel) and imaginary (right panel) parts of matrix χ_{expt}, experimentally obtained through SEQPT and a convex optimization. This is the matrix that characterizes process $\mathcal{E}^{(3)}$. Upper insets show the corresponding values of the target matrix χ_{theo}.

circuits, in contrast with the 36 circuits required by our SEQPT implementation.

To better qualify the performance of the proposed method (SEQPT) for the reconstruction of non-trace-preserving maps, in comparison with the standard accepted one (SQPT), and also to understand the origin of possible errors that are later reflected in fidelity values below 1, we reconstruct the trace-preserving version of $\mathcal{E}^{(3)}$, where the 50% loss subprocess is removed. In addition, other simple processes for $d = 3$, both trace-preserving and non-trace-preserving, are reconstructed: ID (the identity process), ID+LOSS (a 50% loss coupled to the identity process), and the qutrit Hadamard gate H12 and its version with losses H12+LOSS (see Appendix F for the explicit mathematical description of these processes). Table I compares the values of the fidelity of reconstruction for the studied three-dimensional quantum processes. As to highlight, the reconstruction of non-trace-preserving processes through the SEQPT differs by less than 3% from reconstruction using SQPT. Besides, the reconstruction of non-trace-preserving processes results in a slightly lower fidelity than the reconstruction of their trace-preserving counterparts (in the absence of the LOSS subprocess). This drop in the fidelity value could be attributed to the additional number of gates needed to implement the loss of the target process.

B. Process matrix reconstruction: bipartite case $d = 6$

The advantages of the SEQPT method with respect to the SQPT become more evident in higher dimensions. In that regard, we experimentally study the reconstruction of channel $\mathcal{E}^{(6)}$. In this dimension ($d = 6$), we can also

TABLE I. Summary of the fidelities of reconstruction for different non-trace-preserving processes (NTP) and their trace-preserving (TP) counterparts in $d = 3$.

Process fidelity		TP process		NTP process	
		SEQPT	SQPT	SEQPT	SQPT
$d = 3$	ID	0.971	0.982	0.958	0.964
	H01	0.970	0.981	0.956	0.974
	H12	0.953	0.973	0.934	0.954

assess the viability of the non-trace-preserving version of the SEQPT for the general case, when the dimension of the Hilbert space is not a power of a prime number.

We start by performing the full reconstruction of the selected target channel, on the IBMQ processor. For this, the $36 \times 36 = 1296$ coefficients of the χ_{theo} matrix are estimated by sampling all the elements in the tensor product of 2-design $X_{\otimes} = X_1 \otimes X_2$. As in the case $d = 3$, due to the particular relation between the selected basis of the operator and the product of the 2-design, many of the circuits to perform the sampling are repeated. Thus, with this choice, the full reconstruction under the SEQPT method requires the implementation of only 432 different circuits, like that in Fig. 5, out of a total of about $36 \times 36 \times 72 \times 4 = 373\,248$ that would certainly lead to redundancy of measurements. Finally, the statistics over 8192 repetitions of each circuit is collected to obtain the required survival probabilities $\bar{F}_{\otimes}(\mathcal{E}_{j_1 j_2}^{i_1 i_2})$.

The bar plots in Fig. 7(a) indicate the absolute values of the coefficients of the theoretical matrix χ_{theo} (left) and the experimentally reconstructed one χ_{expt} (right). Besides, in Fig. 7(b) we show gray-level map detail of the 11×11 nonzero elements in χ_{theo}, comparing the real (upper panels) and imaginary (lower panels) parts of its coefficients (left panels) with the corresponding coefficients of χ_{expt} (right panels). In this case, we obtain a value for the process fidelity $\mathcal{F}_{\text{SEQPT}} = 0.913$, while for the same process reconstructed with SQPT, which requires a total of 972 circuits, we obtain a slightly lower fidelity, $\mathcal{F}_{\text{SQPT}} = 0.871$. Besides, if the process is assumed to be trace preserving, the standard SEQPT method results in a reconstruction fidelity of only 0.838.

Given that the *a priori* information of the $\mathcal{P}$ matrix is used to experimentally estimate, individually, any coefficient of matrix χ_{theo} of the non-trace-preserving target process $\mathcal{E}^{(6)}$, it is important to check that the obtained results are compatible with that initial assumption. In Fig. 8(a), we show a color map representing the values of the coefficient of the $\mathcal{P}$ matrix in its diagonal form, and in Fig. 8(b), the corresponding values obtained after the full reconstruction from Eq. (8). It can be seen that some elements in the diagonal are slightly greater than 1 (up to 14%), which indicates that the process is not physical. Even so, there
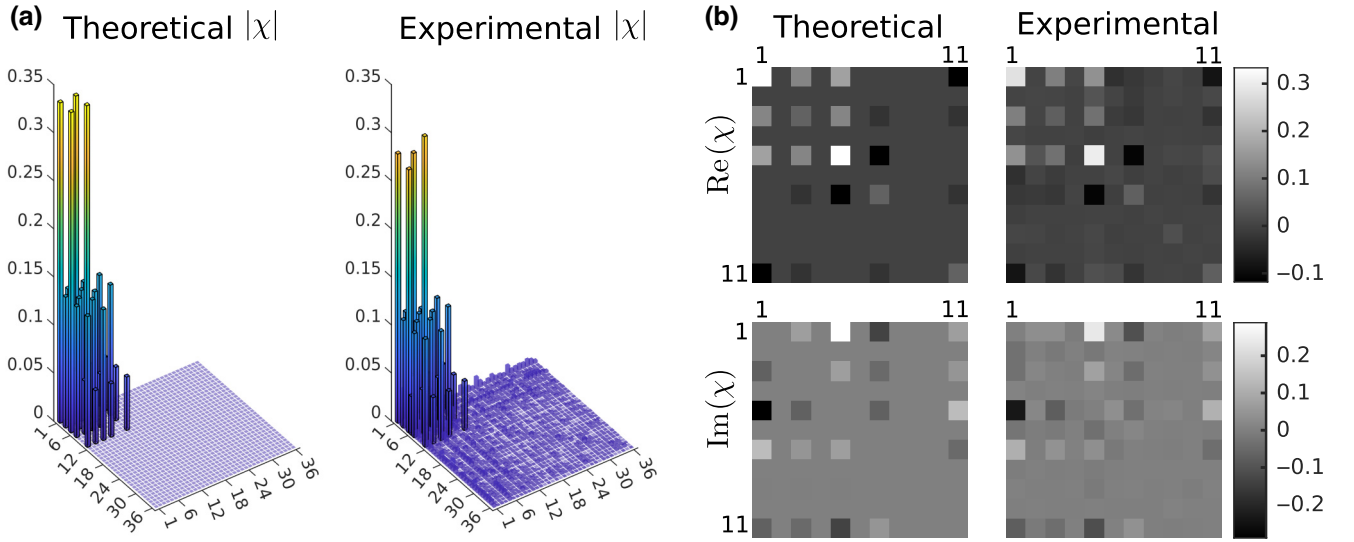
FIG. 7. (a) Comparison of the absolute values of the elements of χ_{theo} and χ_{expt} for the NTP process $\mathcal{E}^{(6)}$, measured on a five-qubit computer from the IBMQ network. (b) Detail of the first 11 basis elements. These elements correspond to the nonzero block in the theoretical matrix [upper left block in the theoretical plot of (a)]. The gray-level map shows the real and imaginary parts for the theoretical and experimental reconstructed matrices.

is a clear similarity with the $\mathcal{P}$ matrix of the target process. Finally, in Fig. 8(c), we show the $\mathcal{P}$ matrix obtained from the postprocessed data, i.e., after convex optimization [see Eqs. (18)]. Although the constraint in the optimization stage is on $\text{Tr}(\mathcal{P})$, the value of each of its elements is very close to that of the nominal process (less than a 4% difference).

For a wider analysis of performance, we also implement and experimentally reconstruct the trace-preserving counterpart of $\mathcal{E}^{(6)}$, where the loss subprocess is removed, and other simple processes in $d = 6$: PHASE (a phase shift of $\pi/3$ on the elements $|1\rangle$ and $|4\rangle$) and PHASE+LOSS (similar to PHASE, but with an additional 50% loss). The explicit Kraus operators for these processes are presented in Appendix F. The comparison of both reconstruction
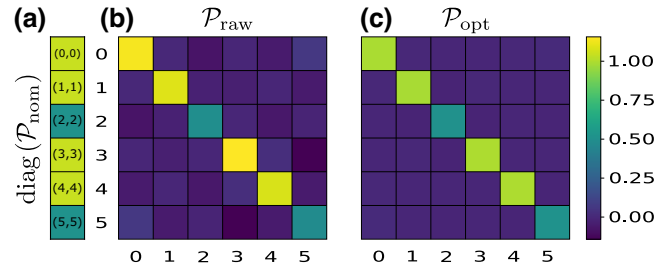
methods, summarized in Table II, shows that the difference in the fidelity values is, in all these cases, less than 1%.

C. Efficiency

As mentioned in Sec. I, a remarkable feature of the SEQPT method is that it is both *selective* and *efficient*. This makes the protocol ideally suited for reconstructing quantum channels that have only a few nonzero elements in its matrix χ. For example, if χ has K nonzero elements, it is possible to reconstruct only these elements (*selectivity*), and with a number of evaluation circuits that scales with K, independently of the dimension d of the Hilbert space (*efficiency*) [22]. In contrast, the SQPT method reconstructs the entire matrix for which it requires a number of circuits that quickly grows with the dimension as about d^4.

To perform an efficient reconstruction of the matrix element χ_j^i, one must appeal to the fact that the mean fidelities $\bar{F}_\otimes(\mathcal{E}_j^i)$ and $\bar{F}_k(\mathcal{E}_j^i)$ ($k = 1, 2$) can be estimated by averaging the survival probabilities of a random subset of states

FIG. 8. Comparison between the diagonal form of the nominal $\mathcal{P}$ matrix and the experimentally reconstructed one. (a) Diagonal of the $\mathcal{P}$ matrix for the nominal process $\mathcal{E}^{(6)}$. (b) Full $\mathcal{P}$ matrix obtained for the process reconstructed by the NTP version of the SEQPT method. (c) The $\mathcal{P}$ matrix for the process postprocessed by the convex optimization routine.

TABLE II. Summary of the fidelities of reconstruction for different NTPs and their TP counterparts in $d = 6$.

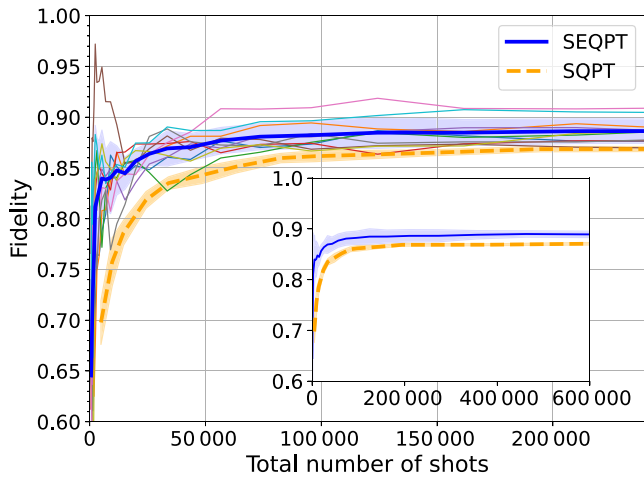| Process fidelity		TP process		NTP process	
		SEQPT	SQPT	SEQPT	SQPT
$d = 6$	ID	0.950	0.947	0.930	0.938
	PHASE	0.949	0.945	0.930	0.939
	SWAP25	0.906	0.908	0.913	0.871

FIG. 9. Process fidelity between the nominal quantum process $\mathcal{E}^{(6)}$ and the reconstructed one for an increasing number of shots. Each thin solid line corresponds to a different random sampling of elements in $X_{\otimes}$. The sampling is performed to reconstruct the 25 nonzero elements of the target process matrix χ_{theo} from SEQPT. The thick solid line corresponds to the mean process fidelity among those ten different samplings, while the shaded area represents one standard deviation. For comparison, the mean process fidelity and standard deviation for ten realizations of the SQPT full reconstruction are displayed.

in $X_{\otimes}$, through the modified channel $\mathcal{E}_j^i$, instead of performing the complete sum in Eqs. (B1)–(B3) in Appendix B. At each sampling step m, an element $|\psi_m\rangle$ of $X_{\otimes}$ is randomly chosen (with replacement), the corresponding circuit to estimate the survival probabilities of this quantum state is executed once (one *shot*), and the outcome is used to update the values of $\bar{F}_{\otimes}(\mathcal{E}_j^i)$ and $\bar{F}_k(\mathcal{E}_j^i)$. These estimates improve iteratively as the number of sampling steps m grows. In this way, we carry out the reconstruction of the 25 nonzero elements of the target matrix χ_{theo}, which we previously reconstructed completely (Fig. 7).

Figure 9 shows the process fidelity $\mathcal{F}$ between the target and the reconstructed processes, as a function of the total number of shots for both the SEQPT method and the traditional SQPT method. Each thin line represents a realization of this SEQPT protocol, i.e., the reconstruction of the 25 nonzero elements of χ_{theo} from a particular random sampling of m elements in $X_{\otimes}$ ($m \leq 240 \times 10^3$, or about 10×10^3 *shots* per nonzero matrix element). The thick solid line and shaded area represent the mean value of $\mathcal{F}_{\text{SEQPT}}$ resulting from ten realizations, and its standard deviation, respectively. To compute this fidelity, the remaining elements of the experimental matrix, not measured in this case, are assumed to be zero in accordance with what is expected theoretically, and the resulting process matrix, χ_{raw}, is optimized to ensure its physicality according to Eqs. (18). The inset of Fig. 9 displays the

results from a larger sampling (m up to 600×10^3, or 24×10^3 samples for each nonzero matrix element).

On the other hand, the thick dashed line and shaded area in Fig. 9 represent the mean value of $\mathcal{F}_{\text{SQPT}}$ for the SQPT method, resulting from ten realizations and its standard deviation, respectively. For a given realization, each of the 972 required circuits is executed an increasing number of times, and the corresponding fidelity $\mathcal{F}_{\text{SQPT}}$ is updated with the increasing statistic.

In the SEQPT reconstruction we can see that the mean fidelity value increases quickly with the number of sampled states, reaching a stable value of 0.889. Ideally, this value should be about 1, if only statistical errors are considered. However, the readout fidelity of the ibmq_lima quantum computer, which accounts for the readout error, is estimated to be only 0.938. It should also be noted that the limit value that reaches the mean fidelity is slightly lower than the fidelity value obtained when a full reconstruction of the process is done by the same method ($\mathcal{F}_{\text{SEQPT}} = 0.913$). As described in Sec. IV A, in that case the readout error can be mitigated, after a calibration in the canonical basis, by postprocessing the distribution probability of the outcomes of each circuit. In the present case, we run each circuit only one time: since an individual shot does not represent the complete probability distribution for the circuit, it cannot be mitigated with the standard routine provided by the Qiskit framework module. In the future, an iterative scheme, where the probability distribution of each circuit is estimated with every new shot, could be envisioned to improve the reconstruction quality.

Finally, we can see that an m up to 30×10^3 (about 1200 samples per nonzero matrix element) is enough for a process fidelity whose value differs within 2.5% of its stable value. For comparison, in the SQPT at least $50 \times^3$ total shots are needed to achieve a fidelity value within 2.5% of its stable value. To contextualize this difference, for such precision, the total running time in the IBMQ processor is 9 s for the SEQPT, i.e., it is 67% faster than SQPT, which takes 15 s. Furthermore, what is more important, in sharp contrast to the SQPT, is that the execution time of the SEQPT method will not increase when the dimension d increases, since to fix precision, m should be increased only if the number of nonzero elements in the process matrix is greater [13,22].

V. CONCLUSIONS

In this work, we present a generalization of the SEQPT protocol for non-trace-preserving maps. The proposed method, which works for arbitrary dimensions, uses the *a priori* information of the loss matrix to reconstruct individual elements of the process matrix. To test this scheme, we realize an experimental implementation of the method on a five-qubit superconducting IBM quantum processor. We

successfully reconstruct several processes both in prime-power dimension ($d = 3$) where a state 2-design is known, and in dimensions where this does not occur ($d = 6$).

On the one hand, we show that it is possible to efficiently reconstruct non-trace-preserving processes, with high precision, within the readout error of the current quantum computers. Since quantum processors are very sensitive to the environment, we have to deal with noisy devices, which makes it relevant to have methods for the reconstruction of quantum processes that save resources and have the ability to account for non-trace-preserving stages.

On the other hand, the implementation of such processes in a superconducting quantum processor is made possible by using the discarded Hilbert subspace to introduce controlled losses, generalizing the type of quantum processes that can be implemented and tested on these computers. In addition, this shows a way to use the qubit-based quantum processor as a test bench for quantum circuits in dimensions that are different from 2^N ($N \in \mathcal{N}$), that is, for *qudit* spaces of arbitrary dimension d.

APPENDIX A: MODIFIED CHANNEL AND SURVIVAL PROBABILITIES

In order to make the protocol experimentally clear, we describe how to interpret the action of the modified channel $\mathcal{E}_j^i$ in terms of the physical channel $\mathcal{E}$. It should be noted that, regardless of the peculiarities of the experimental setup, this is a general description of the circuits that must be implemented to obtain the coefficients of the process matrix χ.

(i) Diagonal case. For $i = j$, the effect of the modified channel $\mathcal{E}_i^i$ on a given state $|\psi\rangle$ is

$$\mathcal{E}_i^i(|\psi\rangle\langle\psi|) = \mathcal{E}(E^i|\psi\rangle\langle\psi|E_i) = \mathcal{E}(E^i P_\psi E_i), \quad \text{(A1)}$$

and the probability that $|\psi\rangle$ survives $\mathcal{E}_i^i$ can be obtained by a projective measurement onto $|\psi\rangle$. This procedure is implemented by the circuit described in Fig. 10(a), whose output estimates the value of $\text{Tr}[P_\psi \mathcal{E}(E^i P_\psi E_i)]$.

(ii) Nondiagonal case. For $i \neq j$, the resulting modified channel is nonphysical. In fact, its effect on a given state
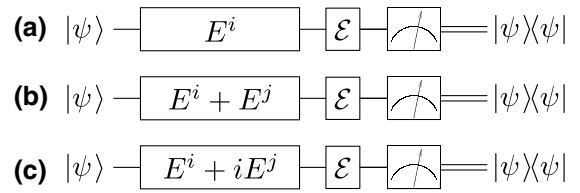

FIG. 10. Schematic of the circuit for measuring the survival probability of state $|\psi\rangle$ through the modified channel $\mathcal{E}_i^i$ [panel (a)] or $\mathcal{E}_j^i$ [panels (b) and (c)]. By sampling these circuits over $|\psi\rangle$ in the state 2-design X, we can estimate any element χ_j^i, corresponding to the process matrix of $\mathcal{E}$.

$|\psi\rangle$ corresponds to

$$\mathcal{E}_j^i(|\psi\rangle\langle\psi|) = \mathcal{E}(E^i|\psi\rangle\langle\psi|E_j) = \mathcal{E}(|\alpha\rangle\langle\beta|) \quad \text{(A2)}$$

with $|\alpha\rangle = E^i|\psi\rangle$ and $|\beta\rangle = E_j|\psi\rangle$. This is equivalent to the action of the original channel $\mathcal{E}$ on matrix $|\alpha\rangle\langle\beta|$, which is not a density matrix, and therefore does not represent a physical state. However, this matrix can always be expressed as a linear combination of *at most* four matrices, each corresponding to one projector. If $|\alpha\rangle$ and $|\beta\rangle$ are orthonormal, $\mathcal{E}(|\alpha\rangle\langle\beta|) = \mathcal{E}(|+\rangle\langle+|) + \mathcal{E}(|-\rangle\langle-|) - [(1 + i)/2](\mathcal{E}(|\alpha\rangle\langle\alpha|) + \mathcal{E}(|\beta\rangle\langle\beta|))$ with $|+\rangle = (|\alpha\rangle + |\beta\rangle)/\sqrt{2}$ and $|-\rangle = (|\alpha\rangle + i|\beta\rangle)/\sqrt{2}$. Even if they are not orthonormal, a similar decomposition exists. Then, the linearity of $\mathcal{E}$ ensures that we can compute the action of the modified channel $\mathcal{E}_j^i$ over any state $|\psi\rangle$ as a linear combination of the action of the original channel $\mathcal{E}$ over a suitable choice of pure states. This implies that an additional operation must be performed on the input state $|\psi\rangle$, as sketched in Figs. 10(b) and 10(c).

Finally, the extension to the bipartite case, where the action of the modified channel on state $|\psi\rangle = |\psi_1\rangle \otimes |\psi_2\rangle \in X_\otimes$ is

$$\mathcal{E}_{j_1 j_2}^{i_1 i_2}(|\psi\rangle\langle\psi|) = \mathcal{E}(E^{i_1 i_2}|\psi\rangle\langle\psi|E_{j_1 j_2})$$
$$= \mathcal{E}(|\alpha\rangle\langle\beta|) \quad \text{(A3)}$$

with $|\alpha\rangle = E^{i_1 i_2}|\psi\rangle = E^{i_1}|\psi_1\rangle \otimes E^{i_2}|\psi_2\rangle$ and $|\beta\rangle = E_{j_1 j_2}|\psi\rangle = E^{j_1}|\psi_1\rangle \otimes E^{j_2}|\psi_2\rangle$, follows from (i) if $i_1 = j_1$ and $i_2 = j_2$ or (ii) if $i_1 \neq j_1$ or $i_2 \neq j_2$, but considering circuits of the type shown in Fig. 2.

APPENDIX B: AVERAGE SURVIVAL FIDELITIES ESTIMATION IN THE BIPARTITE CASE

In the bipartite case, instead of estimating directly the average survival probability $\bar{F}(\mathcal{E}_{j_1 j_2}^{i_1 i_2})$, we first estimate

$$\bar{F}_\otimes(\mathcal{E}_{j_1 j_2}^{i_1 i_2}) = \frac{1}{|X_\otimes|} \sum_{|\psi\rangle \in X_\otimes} \langle\psi|\mathcal{E}_{j_1 j_2}^{i_1 i_2}(|\psi\rangle\langle\psi|)|\psi\rangle. \quad \text{(B1)}$$

The magnitude $\bar{F}_{\otimes}(\mathcal{E}_{j_1 j_2}^{i_1 i_2})$ is the average survival probability over the tensor product of 2-design $X_{\otimes} \equiv \{|\psi_1\rangle \otimes |\psi_2\rangle$ for $|\psi_1\rangle \in X_1, |\psi_2\rangle \in X_2\}$, and $|X_{\otimes}|$ represents the number of elements in the set.

As shown in Ref. [22], the integral that defines $\bar{F}(\mathcal{E}_{j_1 j_2}^{i_1 i_2})$ can be expressed as

$$
\begin{aligned}
\bar{F}(\mathcal{E}_{j_1 j_2}^{i_1 i_2}) = \frac{1}{d+1} \Big\{ &\bar{F}_{\otimes}(\mathcal{E}_{j_1 j_2}^{i_1 i_2})(D_1 + 1)(D_2 + 1) \\
&+ \frac{2}{d} \text{Tr}\Big[\Big(\sum_{\mu\nu} \chi_\mu^\nu E^\nu E_\mu\Big) E^i E_j\Big] \\
&- \bar{F}_1(\mathcal{E}_{j_1 j_2}^{i_1 i_2})(D_1 + 1) - \bar{F}_2(\mathcal{E}_{j_1 j_2}^{i_1 i_2})(D_2 + 1)\Big\},
\end{aligned}
$$
(B2)

where the values of $\bar{F}_1(\mathcal{E}_{j_1 j_2}^{i_1 i_2})$ and $\bar{F}_2(\mathcal{E}_{j_1 j_2}^{i_1 i_2})$ can be seen as the reduced survival probabilities, averaged over the 2-design states X_1 and X_2, respectively:

$$
\bar{F}_k(\mathcal{E}_{j_1 j_2}^{i_1 i_2}) = \frac{1}{D_{k'}|X_k|} \sum_{|\psi_k\rangle \in X_k} \text{Tr}[(P_{\psi_k} \otimes \mathbb{I}_{k'})\mathcal{E}_{j_1 j_2}^{i_1 i_2}(P_{\psi_k} \otimes \mathbb{I}_{k'})]
$$
(B3)

with $k, k' = 1, 2$ and $k \neq k'$.

Thus, the *selectivity* of the method is given by the fact that a particular element $\chi_{j_1 j_2}^{i_1 i_2}$ can be determined by calculating the three mean fidelities $\bar{F}_{\otimes}$, $\bar{F}_1$, and $\bar{F}_2$, over the modified channel $\mathcal{E}_{j_1 j_2}^{i_1 i_2}$.

APPENDIX C: DERIVATION OF THE SEQPT PROTOCOL FOR NON-TRACE-PRESERVING MAPS IN THE BIPARTITE CASE $X_{\otimes} = X_1 \otimes X_2$

Let us consider a product Hilbert space $\mathcal{H} \equiv \mathcal{H}_1 \otimes \mathcal{H}_2$ of dimension d. We start by defining the average over the Haar measure of the product of two operators A and B as

$$
\langle A, B \rangle \equiv \int_{\mathcal{H}} d\psi \, \text{Tr}[P_\psi A P_\psi B],
$$
(C1)

where $P_\psi \equiv |\psi\rangle\langle\psi|$ and the integral is performed using the Haar measure over $\mathcal{H}$. We also define the product average

$$
\langle A, B \rangle_{\otimes} \equiv \int_{\mathcal{H}_1}\int_{\mathcal{H}_2} d\psi_1 d\psi_2 \text{Tr}[P_{\psi_1\psi_2} A P_{\psi_1\psi_2} B],
$$
(C2)

where $P_{\psi_1\psi_2} \equiv P_{\psi_1} \otimes P_{\psi_2} = |\psi_1\rangle\langle\psi_1| \otimes |\psi_2\rangle\langle\psi_2|$, and the integrals are performed over the Haar measure of each

subsystem. Besides, the reduced averages are defined as

$$
\langle A, B \rangle_1 \equiv \int_{\mathcal{H}_1} d\psi_1 \text{Tr}\Big\{ P_{\psi_1} \text{Tr}_2\Big[A\Big(P_{\psi_1} \otimes \frac{\mathbb{I}_2}{D_2}\Big)B\Big]\Big\},
$$
(C3)

$$
\langle A, B \rangle_2 \equiv \int_{\mathcal{H}_2} d\psi_2 \text{Tr}\Big\{ P_{\psi_2} \text{Tr}_1\Big[A\Big(\frac{\mathbb{I}_1}{D_1} \otimes P_{\psi_2}\Big)B\Big]\Big\},
$$
(C4)

where, for $k = 1, 2$, $\mathbb{I}_k$ indicates the identity operator acting on $\mathcal{H}_k$, Tr_k is the partial trace over subsystem $\mathcal{H}_k$, D_k is the dimension of $\mathcal{H}_k$, and the integrals are performed using the Haar measure of the corresponding Hilbert space.

On the one hand, we take into account the expression developed in Refs. [22,45], which relates the four averages defined above:

$$
\begin{aligned}
\langle A, B \rangle = \frac{1}{d+1}\Big[&(D_1 + 1)(D_2 + 1)\langle A, B \rangle_{\otimes} + \frac{2}{d}\text{Tr}[AB] \\
&- (D_1 + 1)\langle A, B \rangle_1 - (D_2 + 1)\langle A, B \rangle_2\Big].
\end{aligned}
$$
(C5)

On the other hand, we consider the average fidelity of a channel $\mathcal{E}$, defined as

$$
\bar{F}(\mathcal{E}) \equiv \int_{\mathcal{H}} d\psi \, \text{Tr}[P_\psi \mathcal{E}(P_\psi)],
$$
(C6)

as well as the average product fidelity

$$
\bar{F}_{\otimes}(\mathcal{E}) \equiv \int_{\mathcal{H}_1}\int_{\mathcal{H}_2} d\psi_1 d\psi_2 \text{Tr}[P_{\psi_1\psi_2}\mathcal{E}(P_{\psi_1\psi_2})],
$$
(C7)

and the average reduced fidelities

$$
\bar{F}_1(\mathcal{E}) \equiv \int_{\mathcal{H}_1} d\psi_1 \text{Tr}\Big\{ P_{\psi_1} \text{Tr}_2\Big[\mathcal{E}\Big(P_{\psi_1} \otimes \frac{\mathbb{I}_2}{D_2}\Big)\Big]\Big\},
$$
(C8)

$$
\bar{F}_2(\mathcal{E}) \equiv \int_{\mathcal{H}_2} d\psi_2 \text{Tr}\Big\{ P_{\psi_2} \text{Tr}_1\Big[\mathcal{E}\Big(\frac{\mathbb{I}_1}{D_1} \otimes P_{\psi_2}\Big)\Big]\Big\}.
$$
(C9)

Recalling the expansion in Eq. (6), and given that each average $\langle\cdot, \cdot\rangle_\xi$ is bilinear in its arguments, we can write

$$
\bar{F}_\xi(\mathcal{E}_{j_1 j_2}^{i_1 i_2}) = \sum_{\substack{\mu_1\mu_2 \\ \nu_1\nu_2}} \chi_{\nu_1\nu_2}^{\mu_1\mu_2} \langle E^{i_1 i_2} E_{\mu_1\mu_2}, E^{\nu_1\nu_2} E_{j_1 j_2} \rangle_\xi,
$$
(C10)

where ξ codifies which of the four fidelities defined in Eqs. (C6)–(C9), and which of the four averages in Eqs.

(C1)–(C4), we are referring to. From this identity and the relation in Eq. (C5), we obtain

$$\bar{F}(\mathcal{E}_{j_1j_2}^{i_1i_2}) = \frac{1}{d+1}[(D_1+1)(D_2+1)\bar{F}_\otimes(\mathcal{E}_{j_1j_2}^{i_1i_2})$$

$$+\frac{2}{d}\mathrm{Tr}(\mathcal{P}E^{i_1i_2}E_{j_1j_2})$$

$$-(D_1+1)\bar{F}_1(\mathcal{E}_{j_1j_2}^{i_1i_2})$$

$$-(D_2+1)\bar{F}_2(\mathcal{E}_{j_1j_2}^{i_1i_2})].\qquad\text{(C11)}$$

Resorting to Eq. (10), the left-hand side of the above equation can be related to the matrix coefficients, to arrive at the desired result:

$$\chi_{j_1j_2}^{i_1i_2} = \bar{F}_\otimes(\mathcal{E}_{j_1j_2}^{i_1i_2})\frac{(1+D_1)(1+D_2)}{d}$$

$$+\frac{1}{d^2}\mathrm{Tr}(\mathcal{P}E^{i_1i_2}E_{j_1j_2}) - \bar{F}_1(\mathcal{E}_{j_1j_2}^{i_1i_2})\frac{1+D_1}{d}$$

$$-\bar{F}_2(\mathcal{E}_{j_1j_2}^{i_1i_2})\frac{1+D_2}{d}.\qquad\text{(C12)}$$

Finally, bearing in mind that each fidelity on the right-hand side of Eq. (C12) is quadratic in P_{ψ_1}, P_{ψ_2}, or $P_{\psi_1\psi_2}$, and defined as a Haar integral over Hilbert spaces with dimensions D_1 and D_2, when such dimensions are powers of a prime number, they can be computed by averaging the integrand over the corresponding 2-designs X_1 or X_2, or over the tensor product 2-design $X_\otimes = X_1 \otimes X_2$, respectively [see Eqs. (B1) and (B3)].

APPENDIX D: BEAM-SPLITTER-LIKE CIRCUIT FOR SIMULATING LOSSES

The loss implemented by the beam-splitter-like gate, which is shown in Fig. 3, can be parameterized through the angle of rotation of the R_z gates. Figure 11 shows the most general form of such a circuit. An argument of $\pi + \phi$ in both of the red colored R_z gates results in the equivalent unitary matrix:

$$U_{\mathrm{bs}} = \begin{pmatrix} 1 & 0 & 0 & 0 \\ 0 & 1 & 0 & 0 \\ 0 & 0 & \cos\phi & -\sin\phi \\ 0 & 0 & \sin\phi & \cos\phi \end{pmatrix}.\qquad\text{(D1)}$$

This can be interpreted as a beam splitter matrix with transmissivity $t = \cos^2(\phi)$ and reflectivity $r = \sin^2(\phi)$. It should be noted that this circuit couples the two-qubit state $|10\rangle \equiv |2\rangle_3$ to the discarded 2-qubit state $|11\rangle \equiv |\ell\rangle$, with a probability equal to r.

APPENDIX E: BASIS OF OPERATORS AND MUBS

To expand each of the channels $\mathcal{E}$ studied in this work, we have chosen, as bases of unitary operators, the well-known Sylvester bases [46,47], which, for any dimension
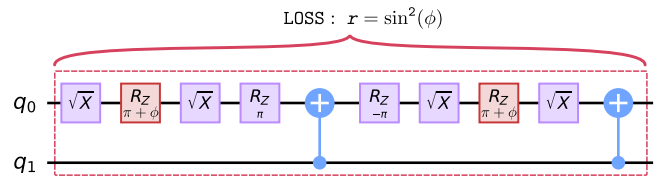

FIG. 11. Circuit to implement a general beam-splitter-like loss affecting state $|10\rangle \equiv |2\rangle_3$. A phase $\pi + \phi$ in both of the red colored R_z gates results in a loss $r = \sin^2(\phi)$ (beam splitter reflectivity).

D, can be written as

$$E_n \equiv E_{kl} = \sum_{m=0}^{D-1} \omega^{ml}|m \oplus k\rangle\langle m|,\qquad\text{(E1)}$$

where $k, l = 0, \ldots, D-1$, $\omega = \exp(2\pi i/D)$ is a root of unity, and "$\oplus$" is the addition modulo D.

For the case $D = D_1 = 2$, the four operators are the Pauli operators together with the identity operator

$$E_{00} = \mathbb{I}_2, \qquad E_{01} = \sigma_z, \qquad E_{10} = \sigma_x, \qquad E_{11} = i\sigma_y,\qquad\text{(E2)}$$

from which we can obtain three Abelian sets of two elements each: $\{E_{00}, E_{01}\}$, $\{E_{00}, E_{10}\}$, and $\{E_{00}, E_{11}\}$. The three bases that diagonalize each of these sets, formed by eigenvectors of the Pauli operators, not only give a complete set of MUBs for D_1 (and, hence, an appropriate 2-design for $\mathcal{H}_1$) but also have the property that the action of any of the four operators, E_{kl}, over any of the elements in the 2-design gives another element within the same MUB basis, except for a global phase. In fact, if $|\psi_M^J\rangle$ is one of the D elements within the J MUB, the following property is verified:

$$E_{kl}|\psi_M^J\rangle = e^{i\alpha(k,l,M,J)}|\psi_{M'}^J\rangle.\qquad\text{(E3)}$$

Analogously, in the case that $D = D_2 = 3$, we can obtain a 2-design by extracting four Abelian subsets from the nine operators E_{kl}. The first of them, $\{E_{00}, E_{01}, E_{02}\}$, is diagonalized by the canonical basis

$$\mathcal{B}_0 = \{|0\rangle, |1\rangle, |2\rangle\} \equiv \{(1,0,0), (0,1,0), (0,0,1)\}.\qquad\text{(E4)}$$

The next set, $\{E_{00}, E_{10}, E_{20}\}$ is diagonalized by

$$\mathcal{B}_1 = \left\{\frac{(1,1,1)}{\sqrt{3}}, \frac{(1,\omega,\omega^2)}{\sqrt{3}}, \frac{(1,\omega^2,\omega)}{\sqrt{3}}\right\},\qquad\text{(E5)}$$

where $\omega = \exp(2i\pi/3)$, $\omega^2 = \omega^*$, and $\omega^3 = 1$. It is clear that $\mathcal{B}_0$ and $\mathcal{B}_1$ are mutually unbiased. Moreover, by choosing $\mathcal{B}_2$ and $\mathcal{B}_3$ as the bases that diagonalize the sets $\{E_{00}, E_{11}, E_{22}\}$ and $\{E_{00}, E_{12}, E_{21}\}$, respectively, we get four MUBs in $D = 3$ and hence a 2-design in the corresponding Hilbert space, $\mathcal{H}_2$. Again, it is easy to check that the property given by Eq. (E3) holds for the nine operators E_{kl}.

APPENDIX F: KRAUS DECOMPOSITION OF THE IMPLEMENTED PROCESSES

All the processes implemented in this work correspond to a Kraus decomposition with a single unitary operator ($\mathcal{E}(\rho) = A\rho A^{\dagger}$). We start by listing those of dimension $d = 3$.

(a) H01: $A = (|0\rangle\langle 0| - |1\rangle\langle 1| + \sqrt{2}|2\rangle\langle 2| + |0\rangle\langle 1| + |1\rangle\langle 0|)/\sqrt{2}$.

(b) H01 + LOSS 50%: $A = (|0\rangle\langle 0| - |1\rangle\langle 1| + |2\rangle\langle 2| + |0\rangle\langle 1| + |1\rangle\langle 0|)/\sqrt{2}$.

(c) H12: $A = (\sqrt{2}|0\rangle\langle 0| + |1\rangle\langle 1| - |2\rangle\langle 2| + |1\rangle\langle 2| + |2\rangle\langle 1|)/\sqrt{2}$.

(d) H12 + LOSS 50%: $A = |0\rangle\langle 0| + |1\rangle\langle 1| - |2\rangle\langle 2| + |1\rangle\langle 2| + |2\rangle\langle 1|)/\sqrt{2}$.

Below, we list the unitary operators corresponding to the processes in $d = 6$.

(a) ID + LOSS 50%: $A = |0\rangle\langle 0| + |1\rangle\langle 1| + |3\rangle\langle 3| + |4\rangle\langle 4| + |2\rangle\langle 2| + |5\rangle\langle 5|)/\sqrt{2}$.

(b) PHASE: $A = (|0\rangle\langle 0| + |3\rangle\langle 3|) + e^{i\pi/3}(|1\rangle\langle 1| + |4\rangle\langle 4|) + (|2\rangle\langle 2| + |5\rangle\langle 5|)$.

(c) PHASE + LOSS 50%: $A = (|0\rangle\langle 0| + |3\rangle\langle 3|) + e^{i\pi/3}(|1\rangle\langle 1| + |4\rangle\langle 4|) + (|2\rangle\langle 2| + |5\rangle\langle 5|)/\sqrt{2}$.

(d) SWAP25: $A = (|0\rangle\langle 0| + |3\rangle\langle 3|) + e^{i\pi/3}(|1\rangle\langle 1| + |4\rangle\langle 4|) + (|2\rangle\langle 5| + |5\rangle\langle 2|)$.

(e) SWAP25 + LOSS 50%: $A = (|0\rangle\langle 0| + |3\rangle\langle 3|) + e^{i\pi/3}(|1\rangle\langle 1| + |4\rangle\langle 4|) + (|2\rangle\langle 5| + |5\rangle\langle 2|)/\sqrt{2}$.

---

[1] C. Outeiral, M. Strahm, J. Shi, G. M. Morris, S. C. Benjamin, and C. M. Deane, The prospects of quantum computing in computational molecular biology, WIREs Comput. Mol. Sci. **11**, e1481 (2020).

[2] GoogleAIQuantum, Hartree-Fock on a superconducting qubit quantum computer, Science **369**, 1084 (2020).

[3] S. K. Liao *et al.*, Satellite-to-ground quantum key distribution, Nature **549**, 43 (2017).

[4] N. Gisin and R. Thew, Quantum communication, Nat. Photon. **1**, 165 (2007).

[5] D. Llewellyn, Y. Ding, I. I. Faruque, S. Paesani, D. Bacco, R. Santagati, Y.-J. Qian, Y. Li, Y.-F. Xiao, M. Huber, M. Malik, G. F. Sinclair, X. Zhou, K. Rottwitt, J. L. O'Brien, J. G. Rarity, Q. Gong, L. K. Oxenlowe, J. Wang, and M. G. Thompson, Chip-to-chip quantum teleportation and multiphoton entanglement in silicon, Nat. Phys. **16**, 148 (2020).

[6] J. B. Altepeter, D. Branning, E. Jeffrey, T. C. Wei, P. G. Kwiat, R. T. Thew, J. L. O'Brien, M. A. Nielsen, and A. G. White, Ancilla-Assisted Quantum Process Tomography, Phys. Rev. Lett. **90**, 4 (2003).

[7] Z.-W. Wang, Y.-S. Zhang, Y.-F. Huang, X.-F. Ren, and G.-C. Guo, Experimental realization of direct characterization of quantum dynamics, Phys. Rev. A **75**, 044304 (2007).

[8] M. Mohseni, A. T. Rezakhani, and D. A. Lidar, Quantum-process tomography: Resource analysis of different strategies, Phys. Rev. A **77**, 032322 (2008).

[9] M. A. Nielsen and I. L. Chuang, *Quantum Computing and Quantum Information* (Cambridge University Press, England, 2000).

[10] A. Bendersky, F. Pastawski, and J. P. Paz, Selective and Efficient Estimation of Parameters for Quantum Process Tomography, Phys. Rev. Lett. **100**, 190403 (2008).

[11] A. Bendersky, F. Pastawski, and J. P. Paz, Selective and efficient quantum process tomography, Phys. Rev. A **80**, 032116 (2009).

[12] C. T. Schmiegelow, M. A. Larotonda, and J. P. Paz, Selective and Efficient Quantum Process Tomography with Single Photons, Phys. Rev. Lett. **104**, 123601 (2010).

[13] C. T. Schmiegelow, A. Bendersky, M. A. Larotonda, and J. P. Paz, Selective and Efficient Quantum Process Tomography without Ancilla, Phys. Rev. Lett. **107**, 100502 (2011).

[14] A. Gaikwad, D. Rehal, A. Singh, Arvind, and K. Dorai, Experimental demonstration of selective quantum process tomography on an NMR quantum information processor, Phys. Rev. A **97**, 022311 (2018).

[15] A. Gaikwad, K. Shende, Arvind, and K. Dorai, Implementing efficient selective quantum process tomography of superconducting quantum gates on IBM quantum experience, Sci. Rep. **12**, 3688 (2022).

[16] C. Dankert, R. Cleve, J. Emerson, and E. Livine, Exact and approximate unitary 2-designs and their application to fidelity estimation, Phys. Rev. A **80**, 012304 (2009).

[17] J. Schwinger, Unitary operator bases, Proc. Natl. Acad. Sci. U.S.A. **46**, 570 (1960).

[18] A. Klappenecker and M. Rötteler, Mutually unbiased bases are complex projective 2-designs, IEEE Int. Symp. Inf. Theory - Proc. **2005**, 1740 (2005).

[19] I. D. Ivonovic, Geometrical description of quantal state determination, J. Phys. A: Math. Gen. **14**, 3241 (1981).

[20] W. K. Wootters and B. D. Fields, Optimal state-determination by mutually unbiased measurements, Ann. Phys. **191**, 363 (1989).

[21] T. Durt, B.-G. Englert, I. Bengtsson, and K. Życzkowski, On mutually unbiased bases, Int. J. Quantum Inf. **8**, 535 (2010).

[22] I. Perito, A. J. Roncaglia, and A. Bendersky, Selective and efficient quantum process tomography in arbitrary finite dimension, Phys. Rev. A **98**, 062303 (2018).

[23] Q. P. Stefano, I. Perito, J. J. Varga, L. Rebón, and C. Iemmi, Experimental characterization of quantum processes: A selective and efficient method in arbitrary finite dimensions, Phys. Rev. A **103**, 1 (2021).

[24] Y. Zheng, C. Song, M. C. Chen, B. Xia, W. Liu, Q. Guo, L. Zhang, D. Xu, H. Deng, K. Huang, Y. Wu, Z. Yan, D. Zheng, L. Lu, J. W. Pan, H. Wang, C. Y. Lu, and X. Zhu, Solving Systems of Linear Equations with a Superconducting Quantum Processor, Phys. Rev. Lett. **118**, 210504 (2017).

[25] E. Knill, R. Laflamme, and G. J. Milburn, A scheme for efficient quantum computation with linear optics, Nature **409**, 46 (2001).

[26] A. Politi, J. C. Matthews, and J. L. O'Brien, Shor's quantum factoring algorithm on a photonic chip, Science **325,** 1221 (2009).

[27] S. Rahimi-Keshari, A. Scherer, A. Mann, A. T. Rezakhani, A. I. Lvovsky, and B. C. Sanders, Quantum process tomography with coherent states, New J. Phys. **13,** 013006 (2011).

[28] Y. Shi and E. Waks, Error metric for non-trace-preserving quantum operations, arXiv:2110.02290.

[29] IBM Quantum, https://quantum-computing.ibm.com/ (2022).

[30] L. Zambrano, L. Pereira, D. Martínez, G. Cañas, G. Lima, and A. Delgado, Estimation of Pure States Using Three Measurement Bases, Phys. Rev. Appl. **14,** 064004 (2020).

[31] S. Satyajit, K. Srinivasan, B. K. Behera, and P. K. Panigrahi, Nondestructive discrimination of a new family of highly entangled states in IBM quantum computer, Quantum Inf. Process. **17,** 212 (2018).

[32] B. K. Behera, S. Seth, A. Das, and P. K. Panigrahi, Demonstration of entanglement purification and swapping protocol to design quantum repeater in IBM quantum computer, Quantum Inf. Process. **18,** 108 (2019).

[33] The meaning of $\sum_k A_k A_k^\dagger \leq \mathbb{I}$ is that all the eigenvalues of the $\sum_k A_k A_k^\dagger - \mathbb{I}$ matrix are negative.

[34] A state 2-design is a finite set of states $X = \{|\psi_m\rangle, m = 1, \ldots, N\}$ over which the mean value of any function f that is quadratic in P_ψ gives the same mean value as on the set of all possible states in $\mathcal{H}$. That is, $\int_\mathcal{H} d\psi\, f(P_\psi) = \sum_{m=1}^N p_m f(P_{\psi_m})$, where $\{p_m\}_{m=1,\ldots,N}$ is some fixed probability distribution and the integration is performed over the Haar measure. In particular, if the probability distribution is uniform ($p_m = 1/|X| = 1/N$ for all $m = 1, \ldots, N$), X is called a *uniform* 2-design.

[35] It should be noted that there are ways to obtain 2-designs that do not require the existence of a complete set of MUBs. However, in this work we exploit the well-understood protocol based on MUBs.

[36] I. Bongioanni, L. Sansoni, F. Sciarrino, G. Vallone, and P. Mataloni, Experimental quantum process tomography of non-trace-preserving maps, Phys. Rev. A **82,** 042307 (2010).

[37] A. P. Lund and T. C. Ralph, Nondeterministic gates for photonic single-rail quantum logic, Phys. Rev. A **66,** 4 (2002).

[38] F. Bouchard, F. Hufnagel, D. Koutný, A. Abbas, A. Sit, K. Heshami, R. Fickler, and E. Karimi, Quantum process tomography of a high-dimensional quantum communication channel, Quantum **3,** 138 (2019).

[39] Y. Kim, Y. S. Kim, S. Y. Lee, S. W. Han, S. Moon, Y. H. Kim, and Y. W. Cho, Direct quantum process tomography via measuring sequential weak values of incompatible observables, Nat. Commun. **9,** 192 (2018).

[40] Qiskit: An open-source framework for quantum computing (2021).

[41] Y.-M. Di and H.-R. Wei, Elementary gates for ternary quantum logic circuit, arXiv:1105.5485.

[42] D. F. James, P. G. Kwiat, W. J. Munro, and A. G. White, in *Asymptotic Theory of Quantum Statistical Inference: Selected Papers* (World Scientific, Singapore, 2005), p. 509.

[43] G. C. Knee, E. Bolduc, J. Leach, and E. M. Gauger, Quantum process tomography via completely positive and trace-preserving projection, Phys. Rev. A **98,** 062336 (2018).

[44] The optimization problem is solved through the PYTHON library cvxpy [48].

[45] I. Perito, Ph.D. thesis, Facultad de Ciencias Exactas, Universidad de Buenos Aires, 2020.

[46] J. J. Sylvester, (1882), Johns Hopkins University Circulars I: 241-242; ibid II (1883) 46; ibid III (1884) 7–9. Summarized in The Collected Mathematics Papers of James Joseph Sylvester (Cambridge University Press, 1909) v III. (1882).

[47] A. Singh and S. M. Carroll, Modeling Position and Momentum in Finite-Dimensional Hilbert Spaces via Generalized Pauli Operators, arXiv:1806.10134.

[48] S. Diamond and S. Boyd, CVXPY: A python-embedded modeling language for convex optimization, J. Mach. Learn. Res. **17,** 2909 (2016).